Liquid films with high surface modulus moving in tubes: dynamic wetting film and jumpy motion

Isabelle Cantat, Benjamin Dollet
Institut de Physique de Rennes, UMR CNRS 6251, Université Rennes 1,
Bâtiment 11A, Campus de Beaulieu, 35042 Rennes cedex, France.
E-mail: isabelle.cantat@univ-rennes1.fr

May 16, 2012

We investigate the motion through a wet tube of transverse soap films, or lamellae, of high surface dilatationnal modulus. Combining local thickness and velocity measurements in the wetting film, we reveal a zone of several centimeters in length, the dynamic wetting film, which is significantly influenced by a moving lamella. The dependence of this influence length on lamella velocity and wetting film thickness provides a discrimination among several possible surfactant minimal models. A spectacular jumpy mode of unsteady motion of a lamella is also evidenced.

1 Introduction

The motion of a liquid meniscus sliding over a wet wall is ubiquitous in many industrial and biological contexts, among which dip coating [1], bubble or droplet motion in pores (e.g. in enhanced oil recovery) and microfluidic channels [2], foam friction on solid boundaries [3], as well as lung diseases [4]. The problem has first been studied by Landau and Levich [5] and Derjaguin [6] (LLD) for a solid plate pulled out of a liquid bath at small velocity. For pure liquids, the dynamics is controlled by the dynamic meniscus that forms between the static meniscus and the wetting film withdrawn by the plate. The LLD model leads to a wetting film thickness $h_{\mathrm{LLD}} = 0.945 \ell_c \mathrm{Ca}^{2/3}$, with ℓ_c the capillary length and $\mathrm{Ca} = \eta U / \gamma$ the capillary number (γ: surface tension, η: liquid viscosity, and U: plate velocity); the extension of the dynamic meniscus along the plate scales like $L_{\mathrm{LLD}} \sim \ell_c \mathrm{Ca}^{1/3}$. These predictions are based on the lubrication approximation $h_{\mathrm{LLD}}/L_{\mathrm{LLD}} \ll 1$, and on a free shear boundary condition at the air/liquid interface.

If the liquid phase is a solution of surfactants, the interfacial stress depends on the surface concentration of surfactants Γ and on the rheology of the surfactant layer. This stress reacts against the local area variation of the interface, with a dependence quantified by a surface dilatational modulus E. The friction against a wall of foams made of solutions with high E is well predicted by the limiting case of a locally incompressible interface [3]: the whole interface then moves with the foam, resulting into a strong shearing of the wetting film between the foam and the wall. For single bubbles and foams, the total interface area of each bubble is constant during the motion, which is compatible with the local incompressibility of the interface.

In other geometries, like dip coating or motion of a lamella (a soap film across a tube), the total area of each connected part of the interface varies, and the location and extension of the zone where area variations occur becomes a central question. A classical assumption is that the area variations are localized in the static meniscus, and that, in contrast with the model by Denkov *et al.* [3], the interface of the wetting film and of the dynamic meniscus move with the plate. The hydrodynamical problem is then governed by the same equations as for pure liquids, after a well adapted rescaling [7]. Several models go beyond these limiting cases, by including surfactant adsorption/desorption [8], diffusion in the bulk [9] or an intrinsic surface viscosity [10]. Recently, the full problem was numerically solved without the lubrication approximation, which allowed to include the whole meniscus into the simulation, with surface diffusion [11] or surface diffusion and adsorption/desorption [12]. However, no clear experimental evidence allows to discriminate between these different models.

Using a surfactant solution with high surface modulus and low bulk viscosity, we bring the first direct experimental evidence that a lamella moving in a wet tube can push the wetting film over centimetric distances, *i. e.* more than two orders of magnitude larger than $L_{\rm LLD}$. We thus introduce the concept of *dynamic wetting film*. We show that its lateral extension, that we call the *influence length*, depends on the initial film thickness and on the lamella velocity. Moreover, we show that the various processes that may govern the influence length lead to very different scalings, discriminated by our experimental data. Finally, we demonstrate a surprising jumpy behavior at high velocity, where the meniscus intermittently slips over its wetting film.

2 Experimental set-up

Single lamellae are created and pushed at prescribed velocity U in a wetted vertical tube of inner diameter $2a = 8.8$ mm following the method of [13]. In order to maximize E, we use a mixture of sodium lauryl dioxyethylene sulfate, cocoamidopropyl betaine, and myristic acid (MAc) in ultrapure water (solution S_1), or the same with 40% wt glycerol (solution S_2), following the protocol of [14]. The wetting film thickness h is measured by white light interferometry using the commercial spectrometer USB4000 (Ocean Optics). Neglecting multiple reflections within the film, the collected light intensity obeys $I(\lambda) = I_0[\alpha + \beta\cos(4\pi n h/\lambda)]$ with I_0 a reference intensity, $n = 1.33$ the optical index of the solution and λ the wavelength. The film thickness $h_{\rm fib}(t)$ is determined by computing the dominant Fourier component of $I(1/\lambda)$. Assuming a steady film profile in the lamella frame, we set $h(x) = h_{\rm fib}(t_0 - x/U)$, with t_0 the time at which the lamella is in front of the fiber. The direction x is oriented downstream, with $x = 0$ at the lamella position (see Fig.1, right). A camera is synchronized with the spectrometer and records the film shape and velocity (Fig. 1, left).

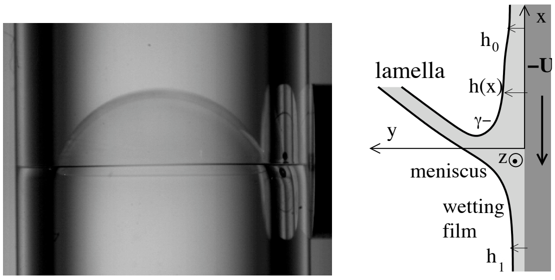

Figure 1: (left) Lamella passing in front of the fiber. (right) Scheme of the meniscus and notations used in the text.

3 Experimental results

Typical wetting film profiles are given on Fig. 2. The signal modulation is destroyed for too high thickness gradients, hence the meniscus profile is not accessible. The wetting film thickness h_0, far ahead the lamella, depends on the time elapsed since the previous lamella has passed. Its evolution by drainage is slow enough for h_0 to remains uniform and constant on the experimental space and time scales, in the range 1 to 20 μm. The thickness h_1 of the film deposited by the lamella does not need to be equal to h_0. If $h_0 \neq h_1$, the meniscus volume changes, but slowly enough for the steady state assumption to remain valid.

Most remarkably, the wetting film begins to swell several centimeters in front of the lamella, at a distance L_0, that we henceforth call the influence length. Some profile shapes are roughly exponential, but the thickest ones display a sharp transition between the flat wetting film and the swollen part of the film close to the meniscus, of typical thickness $h \approx 2h_0$. The rear influence length L_1 is significantly smaller, but still centimetric.

In order to extract L_0 from the experimental data, we have fitted the profile at $x > 0$ by the following phenomenological function, with five fitting parameters: $f(x) = h_0 + [a_3 + a_5(x - a_2)]\{1 - \tanh[(x - a_2)/a_4]\}$. This function was chosen for its compatibility with the main features observed on the experimental profiles. First, since $1 - \tanh[(x - a_2)/a_4] \simeq 2\mathrm{e}^{-2(x-a_2)/a_4}$ at large x, it captures the decay of $h(x)$ towards the flat wetting film of thickness h_0, over a characteristic length scale a_4. Second, for the profiles showing an inflection point, like the two upper curves of Fig. 2, it captures the decrease of $h(x)$ at small x, with a slope a_5, followed by the inflection point at a_2. For the profiles showing no inflection point, like the two lower curves of Fig. 2, the fit works with $a_2 < 0$. We have checked by visual inspection that this fits correctly all experimental data. We have then chosen to define L_0 as $L_0 = a_2 + 2a_4$. Since the rear experimental profiles showed no inflection point, we used a simpler fitting function for $x < 0$: $f(x) = h_1 + a_2' \mathrm{e}^{x/a_3'}$ and we have chosen $L_1 = 2a_3'$.

The length L_0 is plotted as a function of U and h_0 on Fig. 3. The data are somewhat scattered, due to the significant uncertainty on the location of the influence length, since the matching with the flat wetting film is smooth (Fig. 2). Still, they exhibit a clear tendency: L_0 increases with h_0, and decreases with both η and U. A similar trend was obtained for L_1 (data not shown).

In some experiments, the presence of tiny bubbles within the wetting film enabled the simultaneous measurement of the film thickness and of the surface velocity. These bubbles are convected at a velocity $\bar{u}_b = \alpha \bar{u}_s$, with $\bar{u}_s$ the surface velocity (the bar indicating velocities in the laboratory frame) and $\alpha \lesssim 1$ an unknown friction parameter. Comparison with the film thickness profile proves that, as the film begins to swell, the velocity rapidly increases from almost zero to a value of the order of U (Fig. 4). The velocity gradient in the dynamic wetting film is thus close to U/h, and the friction force per unit length (in the z direction)

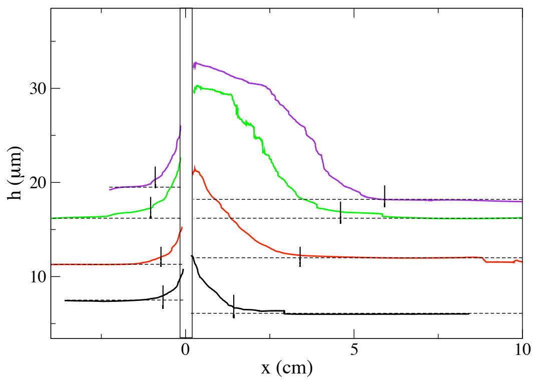

Figure 2: Wetting film profiles obtained with different initial thicknesses and $U = 0.6$ cm/s (solution S_1). The values obtained for L_i and h_i $(i = 0, 1)$ after the profile analysis described in the text are indicated resp. by thick segments and dashed lines. The central box corresponds to the meniscus and $x = 0$ is the lamella position.

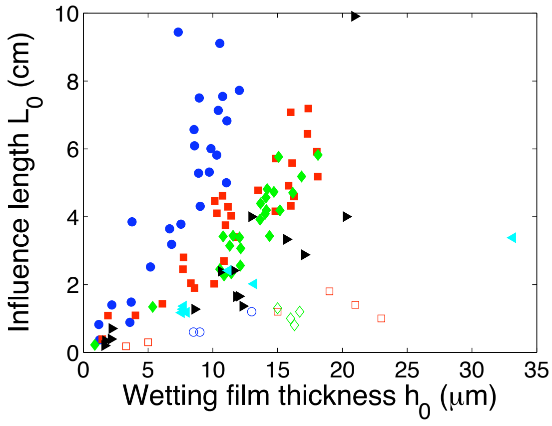

Figure 3: Influence length L_0 as a function of the wetting film thickness h_0 for two bulk viscosities (full symbols: $\eta_{S_1} = 1.0$ mPa·s, open symbols: $\eta_{S_2}, = 4.0$ mPa·s) and various velocities (in cm/s, ○, ●: 0.32, □, ■: 0.60, ◇, ◆: 1.15, ▷, ▶: 2.35, ◁, ◀: 4.20).

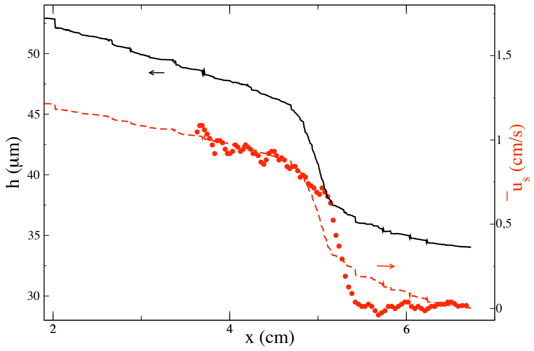

Figure 4: Velocity and thickness profile in the film. (thick line): Film profile obtained with $U = 1.7$ cm/s, S_1, (●): $\bar{u}_s$ measured by tracer tracking for the same experiment, using $\alpha = 0.45$ and (dotted line): $\bar{u}_s$ deduced from the film profile using Eq. (7).

can be estimated as $f_v \approx \eta U(L_0/h_0 + L_1/h_1)$. This estimate, in the range 10 to 30 mN/m for all our experiments, is in good qualitative agreement with the value extracted from the film images (Fig. 1) $f_v = 2\gamma_0 a/R$ [13], with $\gamma_0 = 23.8$ mN/m the equilibrium surface tension [14] and R the radius of curvature of the lamella (data not shown). The friction in the dynamic meniscus alone is given by the Bretherton law $f_{v,B} = 4.70\gamma_0\mathrm{Ca}^{2/3}$ [18] and is at most 1.6 mN/m in our range of velocities. It is thus negligible compared to the dynamic wetting film contribution for this solution.

We also tested a SDS solution, with $\eta = 1.2$ mPa·s and $E < 1$ mN/m and a solution of 12-hydroxy stearic acid with ethanolamine as a counterion [19], with $E = 38$ mN/m and a rheothinning behavior with a high viscosity η varying between 20 and 10^{-2} Pa.s for shear rates between 10^{-2} and 300 s^{-1}. In both cases, no measurable influence length has been observed. This gives a strong hint that a large L_0 is associated to solutions of high E and low η. The influence length results from a competition between the resistance of the surface against compression, and the viscous resistance of the bulk against shear. The former may arise from various microscopic mechanisms, governed by the surface viscosity or elasticity, coupled with the surfactant desorption rate or diffusion. We now investigate them in their simplest form, at the expense of a quantitative modeling; however, this scaling approach appears to be sufficient to identify only one scenario able to capture the main dependencies experimentally observed, in the investigated parameter range.

4 Modelling

In this Section, we first set the equations describing the experimental situation. We then discuss the dimensionless numbers and orders of magnitude of the various parameters involved. Next, we provide a simple analysis of different limits of the full models to obtain different scalings of the influence length, and we compare these scalings to the experiments. Finally, we provide a full numerical simulation of the limiting model which seems the closest to experiments.

4.1 Equations of the problem

We model the region $x > 0$, ahead of the lamella, in the frame of the lamella. We consider a steady regime. Since $h \ll a$, the tube curvature is negligible and we assume an invariance in the z direction. Experiments show that $|\partial_x h| \ll 1$, hence we can apply the lubrication approximation, which simplifies the equation of motion: $0 = -\partial_x p + \eta\partial_{yy}u$, where the pressure p does not depend on y and where u is the x-component of velocity. In this approximation, continuity of normal stress at the interface imposes a Laplace pressure difference: $p - p_0 = -\gamma\partial_{xx}h$, with p_0 the air pressure. The boundary conditions are: $u(y=0) = -U$, and $u(y=h) = u_s$, from which we deduce the velocity profile and the flow rate $q = \int_0^h u\,dy$, which is constant since the flow is incompressible. Since $u = -U$ and $h = h_0$ at $x = \infty$, $q = -Uh_0$, hence:

$$\partial_x(\gamma\partial_{xx}h) = -\frac{6\eta U}{h^2}\left(\frac{2h_0 - h}{h} + \frac{u_s}{U}\right). \qquad (1)$$

Continuity of tangential stress writes:

$$\eta\partial_y u = \partial_x\gamma + \mu^*\partial_{xx}u_s, \qquad (2)$$

where μ^* is the surface viscosity (strictly speaking, $\mu^* = \mu_s + \kappa_s$ is a combination of the surface shear and dilatational viscosities μ_s and κ_s). The surface tension depends on the surface concentration of the surfactants. The surface modulus of a mixture of SLES and CAPB without MAc was shown to be two orders of magnitude lower [14]. Therefore, it is reasonable to assume that $\partial_x \gamma$ is only related to $\partial_x \Gamma_{\mathrm{MAc}}$, hence to use a one-component model. Assuming for simplicity a linear relation for the surface tension:

$$\gamma = \gamma_0 - E\frac{\Gamma - \Gamma_0}{\Gamma_0}, \tag{3}$$

with $\Gamma = \Gamma_{\mathrm{MAc}}$ and Γ_0 the equilibrium surface concentration in MAc. Neglecting surface diffusion, the conservation of surfactants at the interface yields:

$$\partial_t \Gamma + \partial_x (u_s \Gamma) = j, \tag{4}$$

with j the exchange flux from the subphase to the interface. The latter equals the diffusive flux in the subphase, and obeys a kinetic sorption law [21] that we assume linear. Then:

$$j = -D\partial_y c = k\left(c - \frac{\Gamma}{h_\Gamma}\right), \tag{5}$$

at $y = h$, with c the bulk concentration in MAc, c_0 its equilibrium value, $h_\Gamma = \Gamma_0/c_0$, D the diffusion coefficient, and k the sorption velocity, both assumed to be the ones of the micelles in which MAc is solubilized [14]. Finally, the bulk concentration of surfactants obeys the diffusion–convection equation:

$$\partial_t c + u\partial_x c + v\partial_y c = D(\partial_{xx} c + \partial_{yy} c), \tag{6}$$

where v is the y-component of the velocity.

4.2 Dimensionless numbers and orders of magnitude

The film velocity U and the wetting film thickness h_0 naturally fix the orders of magnitude of the velocities and thicknesses. Hence, after (1), the thickness varies significantly over the dynamic meniscus, of length $\ell_{\mathrm{LLD}} = h_0 \mathrm{Ca}^{-1/3}$. The velocities are in the range $U = [5\,10^{-3} - 10^{-1}]$ m/s and the capillary number is thus $\mathrm{Ca} = [2\,10^{-4} - 4\,10^{-3}]$, with $\gamma = 23$ mN/m and $\eta = 10^{-3}$ Pa.s. Since $h_0 \approx 10$ μm in our measurements, $\ell_{\mathrm{LLD}} \approx 10^2$ μm. The dynamic meniscus extension is thus two orders of magnitude shorter than the influence length. Hence, in the influence zone, Laplace pressure is negligible and (1) reduces to:

$$u_s = U\left(1 - \frac{2h_0}{h}\right), \tag{7}$$

in agreement with experimental data shown on Fig. 4. Furthermore, from the continuity of tangential stress (2) and the surface equation of state (3),

$$u(x,y) = \frac{1}{\eta}\left(\mu^* \partial_{xx} u_s - \frac{E}{\Gamma_0}\partial_x \Gamma\right) y - U. \tag{8}$$

A relevant dimensionless number is the Marangoni number, $\mathrm{Ma} = E/\gamma_0$. The coefficient E, as defined in our model, is the ratio between the surface tension variation and the surfacic concentration relative variation. With the oscillating bubble method we measure E_D, the ratio between the surface tension variation and the interface area relative variation. These are the same quantities if the frequency is high enough for the surfactant exchange with the bubble to be negligible. The measure at 0.2 Hz gives $E_{DS} = 110$ mN/m, and $E_{DL} = 285$ mN/m for the storage and loss modulus [14]. Myristic acid alone, deposited on a water surface (at pH 2) in a Langmuir trough, has a very low solubility: the variation of area A is thus directly connected with the surface concentration. It has a higher surface tension (of the order of 50 mN/m at the monolayer collapse) than its mixture with SLES and CAPB, and from the slope of the curve $\gamma(A)$, we estimate its elastic modulus as $E \approx 60$ mN/m [16, 17]. From these different data we can set $E \approx 10^2$ mN/m in our model, and $\mathrm{Ma} \approx 4$.

As underlined by D. Quéré and A. de Ryck [20], the ratio $h_\Gamma = \Gamma_0/c_0$ is an important length scale in the problem. SLES and CAPB are soluble surfactants above their cmc and their equilibration time scales are much smaller than the MAc equilibration time scale. Only the MAc concentration should thus be taken into account to build h_Γ. The MAc maximal surfacic concentration before collapse is known [16, 17], but corresponds to a much higher surface tension ($\gamma = 50$ mN/m) than the tension measured for the surfactant mixture ($\gamma = 23$ mN/m). SLES and CAPB are thus present at the surface and the MAc surfacic concentration is *a priori* unknown. For MAc solution, a measurable variation of surface tension is obtained for surfacic concentration above $\Gamma = 3 \times 10^{-6}$mol/m^2 and the collapse occurs for $\Gamma = 8 \times 10^{-6}$ mol/m^2. We thus set $\Gamma_0 \approx 5 \times 10^{-6}$ mol/m^2. With $c_0 = 0.88$ mol/m^3, the MAc concentration we get $h_\Gamma = \Gamma_0/c_0 = 5$ μm.

If there is a coupling with the bulk concentration, another relevant dimensionless number is the Péclet number $\mathrm{Pe} = h_0 U/D$. The diffusion coefficient is rather difficult to estimate. Diffusivity of short single molecules in water is of the order of 10^{-9} m^2/s. However, the MAc is mainly solubilised in SLES/CAPB micelles [14]. Their size is unknown, but the mixture is transparent and its viscosity is indistinguishable from that of pure water, hence the micelles are likely to be very small. We will thus assume $D \approx 10^{-10}$ m^2/s, leading to $\mathrm{Pe} \approx 10^3$.

Finally, to our knowledge, there is no experimental data on sorption velocities for MAc.

4.3 Scaling analysis

Interfacial stresses build up either due to surface elasticity, or surface viscosity. If the interfacial dynamics was dictated solely by surface viscosity, Eq. (8) would become, for $y = h$ and $E = 0$:

$$1 + \frac{u_s}{U} = \frac{\mu^* h}{\eta U} \partial_{xx} u_s. \tag{9}$$

The thickness and surface velocity profiles can then be solved analytically (see Appendix). From experiments, the variation of u_s is of the order of U (Fig. 4), leading to the scaling:

$$L_{0,v} = \left(\frac{\mu^* h_0}{\eta} \right)^{1/2}, \tag{10}$$

which does not capture the observed dependence of L_0 on the lamella velocity. We henceforth neglect the interfacial viscosity to focus on the other contributions from the surfactants.

We first estimate the surface convection of surfactant term $\partial_x(u_s\Gamma)$. The dynamic wetting film is compressed by the moving lamella, inducing a typical surface concentration increase $\Delta\Gamma > 0$. Hence, $u_s \partial_x \Gamma \sim U\Delta\Gamma/L_0$. Moreover, Eq. (8) leads to: $u_s \sim -U - Eh\partial_x\Gamma/\eta\Gamma_0$, from which we deduce $\Gamma\partial_x u_s \sim -Eh_0\Delta\Gamma/\eta L_0^2$. Therefore, $\Gamma\partial_x u_s / u_s \partial_x \Gamma \sim Eh_0/\eta U L_0$. Experimentally, the latter parameter equals 3 with $h_0 \approx 10^{-5}$ m, $U \approx 1$ cm/s and $L_0 \approx 3$ cm, showing, as expected, that the convective term $\partial_x(u_s\Gamma)$ is dominated by the velocity variation, which tends to accumulate surfactant in front of the lamella. The concentration gradient only reduces this effect. If we neglect this last term, we get the following scaling law, as already obtained in [8]:

$$\partial_x(\Gamma u_s) \sim -\frac{Eh_0\Delta\Gamma}{\eta L_0^2} < 0. \tag{11}$$

This term is balanced in (4) by the exchange term with the bulk j, which obeys (5).

If k is small, the exchange is limited by the desorption kinetics, and $c \simeq c_0$. Then $j \sim -k\Delta\Gamma/h_\Gamma$, hence from (4) and (11):

$$L_{0,a} \sim \left(\frac{Eh_0 h_\Gamma}{\eta k} \right)^{1/2}. \tag{12}$$

This scaling is exactly the same as in the viscous case (10), with an effective surface viscosity $\mu^*_{\text{eff}} = Eh_\Gamma/k$.

If desorption is fast, the surface is in equilibrium with the subphase and, close to the meniscus, the concentration increase in the subphase scales as $\Delta c(h) = \Delta\Gamma/h_\Gamma$. Then we are in a diffusive regime: $j = -D\partial_y c$ at $y = h$. If the gradient is established over the diffusive distance $h_d \sim \sqrt{DL_0/U}$, this leads to the scaling behavior:

$$\begin{aligned} L_{0,d} &\sim \left(\frac{Eh_\Gamma}{\eta} \right)^{2/3} \frac{h_0^{2/3}}{(DU)^{1/3}} \\ &= h_0 \frac{\mathrm{Ma}}{\mathrm{Ca}} \left(\frac{\mathrm{PeCa}}{\mathrm{Ma}} \right)^{1/3} \left(\frac{h_\Gamma}{h_0} \right)^{2/3}, \end{aligned} \tag{13}$$

which agrees qualitatively with the experimental dependencies of L_0 on h_0 and U.

This is only valid if $h_d < h_0$. Injecting (13) in the expression of h_d, we get the condition

$$K = \left(\frac{EDh_\Gamma}{\eta U^2 h_0^2} \right)^{1/3} = \left(\frac{\mathrm{Ma}}{\mathrm{CaPe}} \frac{h_\Gamma}{h_0} \right)^{1/3} < 1\ . \tag{14}$$

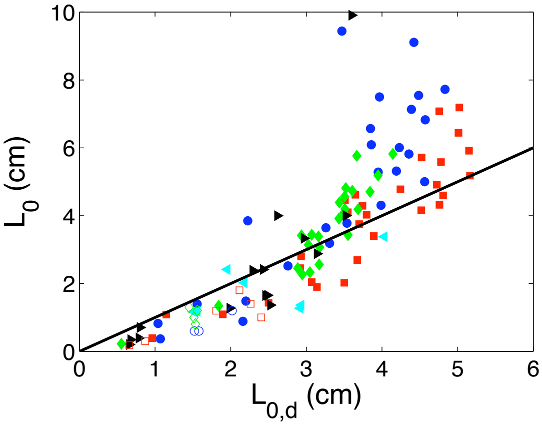

Figure 5: Influence length L_0 as a function of the diffusive length $L_{0,d}$ given by Eq. (13) (full symbols: $\eta_{S_1} = 1.0$ mPa·s, open symbols: $\eta_{S_2}, = 4.0$ mPa·s) and various velocities (in cm/s, ○, ●: 0.32, □, ■: 0.60, ◊, ♦: 1.15, ▷, ▶: 2.35, ◁, ◀: 4.20). The black line corresponds to $L_0 = L_{0,d}$.

With the experimental parameter values (see section 4.2), we get $K \approx 2$. If $h_d \gg h_0$, the gradient $\partial_y c$ becomes small and j is estimated from surfactant conservation: $j = \partial_x \left(\int_0^h ucdy \right) \simeq \partial_x \left(c \int_0^h udy \right)$. From mass conservation, the flow rate $\int_0^h udy$ is a constant, equal to $-Uh_0$. Hence, $j \sim -Uh_0 \Delta c / L_0$, and L_0 in this convective regime is thus governed by:

$$L_{0,c} \sim \frac{Eh_\Gamma}{\eta U} = h_0 \frac{\text{Ma}}{\text{Ca}} \frac{h_\Gamma}{h_0} \, , \tag{15}$$

which does not capture the observed dependence of L_0 on h_0.

Overall, the only regime compatible with our experimental results is the diffusive one. The rescaling by (13) shown in Fig. 5 provides a reasonable agreement with the experimental data, without adjustable parameter. The discrepancy at large L_0 probably arises from nonlinear effects neglected in our simple approach, especially in the relation $\gamma(\Gamma)$.

Moreover, we do not explain why L_1 is significantly shorter than L_0 (Fig. 2); this suggests that the interface resists more compression than extension.

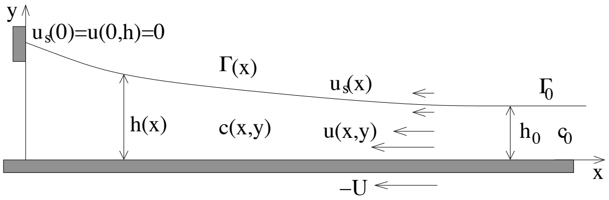

Figure 6: Sketch of the fluid film and notation used in the text.

4.4 Numerical simulation

Here we solve the full model in the diffusive regime, with negligible intrinsic surface viscosity μ^*. We deal with the unsteady equations, as a mean to provide a smooth numerical convergence towards the steady solution.

We have to solve the surfactant mass balance at the interface (4) and in the bulk (6), and mass conservation under the form $\partial_t h = -\partial_x q$. In these equations, u obeys (8) with $\mu^* = 0$. From the continuity equation, $\partial_x u + \partial_y v = 0$, hence $v = Ey^2 \partial_{xx}\Gamma / 2\eta\Gamma_0$.

An important assumption of the model, merely based on experimental evidence, is that the interface moves at the film velocity close to the film, so we impose $u_s(0) = 0$.

The initial conditions are, at $t = 0$: $h = h_0$, $\Gamma = \Gamma_0$, $c = c_0$; and the boundary conditions are, at $x = 0$: $u_s = 0$, *i.e.* $E\, h\, \partial_x \Gamma = -\eta U \Gamma_0$; at $x = \infty$: $h = h_0$, $\Gamma = \Gamma_0$, $c = c_0$; at $y = 0$: $\partial_y c = 0$; at $y = h$: $c = c_0 \Gamma / \Gamma_0$, consistently with the hypothesis of fast desorption.

The variables are rescaled using $t = \alpha h_0 \bar{t} / U$, $y = h_0 \bar{y}$, $h = h_0 \bar{h}$, $x = \alpha h_0 \bar{x}$, $\Gamma = \Gamma_0 \bar{\Gamma}$, $c = c_0 \bar{c}$, with $\alpha = \text{Ma}/\text{Ca}$. Substituting the expressions of the velocities, we get:

$$\begin{aligned} \partial_{\bar{t}} \bar{\Gamma} &= \bar{\Gamma} \partial_{\bar{x}} \bar{\Gamma} \partial_{\bar{x}} \bar{h} + \bar{h} \bar{\Gamma} \partial_{\bar{x}\bar{x}} \bar{\Gamma} + (\partial_{\bar{x}} \bar{\Gamma})^2 \bar{h} + \partial_{\bar{x}} \bar{\Gamma} \\ &\quad - K_1 \partial_{\bar{y}} \bar{c}, \end{aligned} \tag{16}$$

$$\partial_{\bar{t}} \bar{h} = \bar{h} \partial_{\bar{x}} \bar{h} \partial_{\bar{x}} \bar{\Gamma} + \frac{1}{2} \bar{h}^2 \partial_{\bar{x}\bar{x}} \bar{\Gamma} + \partial_{\bar{x}} \bar{h}, \tag{17}$$

$$\begin{aligned} \partial_{\bar{t}} \bar{c} &= \partial_{\bar{x}} \bar{c} + \bar{y} \partial_{\bar{x}} \bar{c} \partial_{\bar{x}} \bar{\Gamma} + \frac{1}{2} \bar{y}^2 \partial_{\bar{y}} \bar{c} \partial_{\bar{x}\bar{x}} \bar{\Gamma} \\ &\quad + \frac{K_1}{K_2} \partial_{\bar{y}\bar{y}} \bar{c} + K_3 \partial_{\bar{x}\bar{x}} \bar{c}, \end{aligned} \tag{18}$$

with dimensionless parameters $K_1 = h_0 \text{Ma} / (\text{Ca}\, \text{Pe} h_\Gamma)$ and $K_2 = h_0 / h_\Gamma$, and the boundary conditions at $t = 0$: $\bar{h} = 1$, $\bar{\Gamma} = 1$,

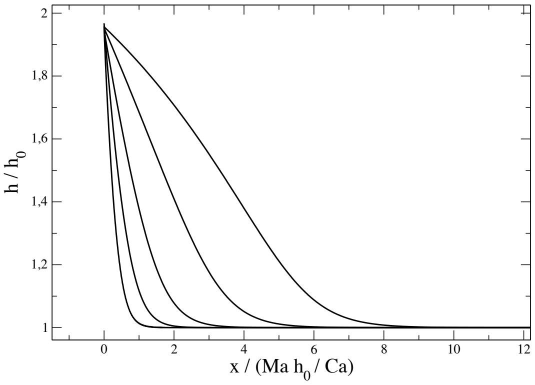

Figure 7: Numerical value of the wetting film thickness in steady regime for $K_1/K_2 = 1$ and $K_1 = [0.42, 0.82, 1.89, 4.35, 10]$ (from top curve to bottom curve).

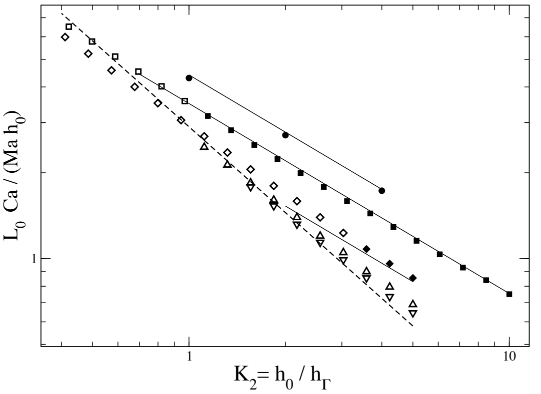

Figure 8: Numerical value of the influence length in steady regime for $K_1/K_2 = 0.5$ (●), 1 (■, □), 3 (◆, ◇), 9 (△) and 18 (▽). The full symbols verify $K_1/K_2^2 < 1$ and are fitted by the law $3.5K_2^{-2/3}(K_1/K_2)^{-1/3}$ (full lines). The open symbols verify $K_1/K_2^2 > 1$ and are fitted by the law $2.9/K_2$.

$\bar{c} = 1$; at $\bar{x} = 0$: $\partial_{\bar{x}}\bar{\Gamma} = -1/\bar{h}$; at $\bar{x} = \infty$: $\bar{h} = 1$, $\bar{\Gamma} = 1$, $\bar{c} = 1$; at $\bar{y} = 0$: $\partial_{\bar{y}}\bar{c} = 0$; at $\bar{y} = \bar{h}$: $\bar{c} = \bar{\Gamma}$. Finally, a condition on $\bar{c}$ is needed at $\bar{x} = 0$: we choose to impose $\partial_{\bar{x}}\bar{c} = 0$.

We solved the equation set (16,17,18) with a finite difference model. The explored parameter range is chosen accordingly to the previous order of magnitude analysis which leads to $K_1 = [0.1 - 40]$; $K_2 = [0.1 - 10]$. The term proportional to K_3 is negligible, but plays an important role to stabilise the numerical scheme. We thus kept it, with an artificial value of $K_3 = 10^{-2}$. This term does not modify the solutions, but suppresses artificial small high frequency oscillations.

The wetting film thickness is roughly exponential for small influence length, but an inflexion point appears at larger influence length. However the plateau is more pronounced experimentally than in the numerical result (see Fig. 2 and 7).

The influence length, defined with the same criterion as for the experimental data, is plotted on Fig. 8 as a function of K_2 for different values of K_1/K_2 and compared to the scaling laws discussed in section 4. The equations (13, 14, 15) predict that if $(K_1/K_2^2)^{1/3} \ll 1$, $L = h_0 \mathrm{Ma}\,(K_2K_1)^{-1/3}/\mathrm{Ca}$, and in the other limit $L = h_0\mathrm{Ma}K_2^{-1}/\mathrm{Ca}$. Both regimes are obtained numerically, and the transition occurs at the expected value. The scaling approach is thus robust and the full resolution confirms the power law predictions in the diffusive and convective regimes.

5 Unsteady regime

Finally, the most deformed lamellae deviate from steady motion by a striking scenario: they undergo periodic "jumps" between phases of constant velocity (Fig. 9). These jumps are quick (less than 10 ms) and macroscopic (of order 1 mm), which make them easily observable by naked eye. The curvature is partially released during jumps, and builds up again during the phases of constant velocity. Integrating Eq. (2) (with $\mu^* = 0$) along the front part of the dynamic wetting film yields $\gamma_- = \gamma_0 - \int_0^\infty \eta\partial_y u \mathrm{d}x \sim \gamma_0 - \eta U L_0/h_0$, with γ_- the value of the surface tension close to the meniscus. The largest values obtained for UL_0/h_0 are close to γ_0, which shows that surface tension significantly decreases towards the meniscus. It is likely that the interface becomes unstable below a certain value of γ_- and collapses as in Langmuir monolayers [22], and that the jumps are macroscopic manifestations of such an instability. This unsteady behavior is in marked contrast with that of SDS films, which never showed such jumps [13].

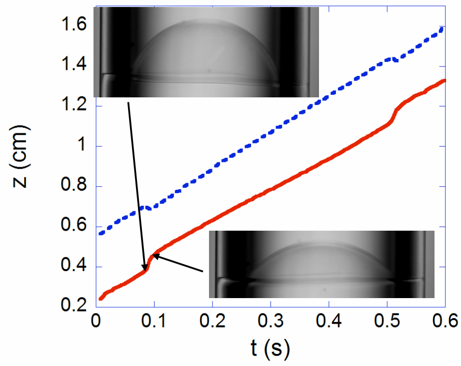

Figure 9: Time evolution of the position of the meniscus (plain line) and of the leading point of the lamella (dashed line), in the laboratory frame and in the jumpy regime. Two snapshots show the shape of the lamella just before, and just after, a jump.

6 Conclusion

As a conclusion, we have identified the influence length L_0 over which an air/liquid interface of a wetting film is entrained by a lamella. We have quantified its dependencies on the lamella velocity, the wetting film thickness and the viscosity. We have shown that such a experimental characterisation helps discriminating between different surfactant models; this may be helpful, since not many experimental observations enable to discriminate among the various surfactant processes.

Furthermore, our study may provide a quantitative criterion for the transition between tangentially immobile and mobile interfaces in foam/wall friction [3]. With ℓ a typical bubble size, these two limits correspond respectively to $L_0 \gg \ell$ and $L_0 \ll \ell$, and the transition criterion $L_0 = \ell$ may be expressed from our predictions, in terms of the material parameters of the surfactants. Experimental tests of this hypothesis are under way.

7 Appendix: analytical solution with surface viscosity

In this Appendix, we derive an analytical solution in the case where interfacial dynamics is dictated solely by surface viscosity. Although this limit is rarely met in practice [10], and in particular not in our experiments, it is a simple way to quantify the influence of surfactants, since it does not require to solve the concentration fields; surface viscosity can then be thought as an effective parameter mimicking more complex surfactant dynamics [23].

After (9), $\partial_{xx} u_s = \eta U(1 + u_s/U)/\mu^* h$, hence after (7), the surface velocity obeys a differential equation: $\partial_{xx} u_s = \eta U(1 - u_s^2/U^2)/2\mu^* h_0$, with boundary conditions: $u_s = -U$ at $x = \infty$, and $u_s = 0$ at $x = 0$. We use the rescaling: $\omega = (u_s + U)/U$ and $\xi = x/L_{0,v}$ with $L_{0,v}$ given by (10) to obtain:

$$\partial_{\xi\xi}\omega = \omega - \frac{\omega^2}{2}, \qquad (19)$$

with $\omega = 0$ at $\xi = \infty$, and $\omega = 1$ at $\xi = 0$.

Multiplying (19) by $2\partial_\xi \omega$ and integrating, we get: $(\partial_\xi \omega)^2 = \omega^2 - \omega^3/3$, the additive constant being dropped since $\partial_\xi \omega = 0$ at $\xi = \infty$. Since ω is expected to be a decreasing function of ξ from the boundary conditions, we have therefore: $\partial_\xi \omega = -\omega\sqrt{1 + \omega/3}$. Integrating once more and using the condition at $\xi = 0$, we get the velocity profile:

$$\omega(\xi) = 3\left\{1 - \left[\frac{(1+\sqrt{2/3})e^{\xi} - 1 + \sqrt{2/3}}{(1+\sqrt{2/3})e^{\xi} + 1 - \sqrt{2/3}}\right]^2\right\}. \qquad (20)$$

The thickness profile follows from (7). Both profiles are plotted in Fig. 10. The thickness profile is convex, and resembles the two profiles of lowest h_0 in Fig. 2.

Acknowledgements

This project was supported by the Institut Universitaire de France. We thank A. Saint-Jalmes, N. D. Denkov and S. Tcholakova for enlightening discussions.

References

[1] P. G. de Gennes, F. Brochard-Wyart, D. Quéré, *Gouttes, bulles, perles et ondes* (Belin, Paris, 2002).

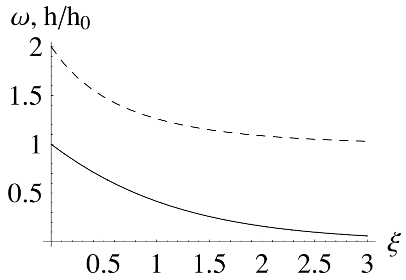

Figure 10: Plot of the rescaled surface velocity ω (plain line), and of the rescaled thickness (dashed line), as a function of the rescaled coordinate ξ.

[2] H. Bruus, *Theoretical Microfluidics* (Oxford University Press, Oxford, 2008).

[3] N. D. Denkov, V. Subramanian, D. Gurovich, A. Lips, *Colloids Surf. A*, 2005, **263**, 129.

[4] J. Goerke, *Biochim. Biophys. Acta*, 1998, **1408**, 79.

[5] L. Landau, B. Levich, *Acta Physicochim. USSR*, 1942, **17**, 42.

[6] B. Derjaguin, *Kolloid Z.*, 1933, **64**, 1.

[7] A. Q. Shen, B. Gleason, G. H. McKinley, H. A. Stone, *Phys. Fluids*, 2002, **14**, 4055.

[8] G. Hirasaki, J. B. Lawson, *Soc. Pet. Eng. J.*, 1985, 176.

[9] J. Ratulowski, H. C. Chang, *J. Fluid Mech.*, 1990, **210**, 303.

[10] B. Scheid, J. Delacotte, B. Dollet, E. Rio, F. Restagno, E. van Nierop, I. Cantat, D. Langevin, H. A. Stone, *EPL*, 2010, **90**, 24002.

[11] C. Pozrikidis, *J. Eng. Math.*, 2001, **41**, 237.

[12] R. Krechetnikov, G. M. Homsy, *J. Fluid Mech.*, 2006, **559**, 429.

[13] B. Dollet, I. Cantat, *J. FLuid Mech.*, 2010, **652**, 529.

[14] K. Golemanov, S. Tcholakova, N. D. Denkov, M. Vethamuthu, A. Lips, *Langmuir*, 2008, **24**, 9956.

[15] C. H. Chang, E. I. Franses, *Colloids Surf. A*, 1995, **100**, 1.

[16] S. Akamatsu, F. Rondelez, *J. Phys. II France*, 1991, **1**, 1309.

[17] J. G. Petrov, T. Pfohl, H. Möhwald, *J. Phys. Chem. B*, 1999, **103**, 3417.

[18] F. P. Bretherton, *J. Fluid Mech.*, 1961, **10**, 166.

[19] A. L. Fameau, A. Saint-Jalmes, F. Cousin, B. Houinsou Houssou, B. Novales, L. Navailles, F. Nallet, C. Gaillard, F. Boué, J. P. Douliez, *Angew. Chem. Int. Ed.*, 2011, **50**, 8264.

[20] D. Quéré, A. de Ryck, *Ann. Phys.*, 1998, **23**, 1.

[21] D. A. Edwards, H. Brenner, D. T. Wasan, *Interfacial Tansport Processes and Rheology* (Butterworth–Heinemann, Boston, 1991).

[22] K. Y. C. Lee, *Annu. Rev. Phys. Chem.*, 2008, **59**, 771.

[23] E. A. van Nierop, B. Scheid, H. A. Stone, *J. Fluid Mech.*, 2008, **602**, 119.